Prospect of High-Field MRI

Hitoshi Wada, Masaki Sekino *Member IEEE*, Hiroyuki Ohsaki *Member IEEE*,
Tatsuhiro Hisatsune, Hiroo Ikehira, and Tsukasa Kiyoshi

Abstract— High-Field MRI provides high resolutions, well-defined chemical shift spectra and large data acquisition rates, and may bring about a paradigm shift in medicine through the *in-vivo* observation of metabolism. An 11.7 T whole body MRI magnet, for example, should be able to observe metabolic reactions occurring in a human body in addition to producing very precise images of body structures. At this field ^{13}C-NMR and biochemical reactions of organic molecules can be detected and analyzed in-situ. Then, organs, tissues, vessels and biochemical processes responsible for irregularities in question will be identified. However, an 11.7 T MRI magnet with a bore diameter of 900 mm is a big challenge to the present magnet technology. Field strengths, magnet sizes and superconducting materials to be needed for future high-field MRI are described.

Index Terms—magnetic resonance imaging, magnetic resonance spectroscopy, NbTi, Nb$_3$Sn, superconducting magnet.

I. INTRODUCTION

AGING of society is the most serious issue many countries confront in the 21st century. To ensure that people can live a comfortable life in such a society, it is necessary to realize human-friendly medicine that can provide medical care suitable to patients in accordance with their individual conditions. It is also required to maintain the physical and mental health of elderly people such that they can participate in society. We believe that non-invasive high-field MRI can be an effective scientific approach to solving such problems in the aging society.

MRI is an abbreviation for Magnetic Resonance Imaging. The first image by MRI was demonstrated in 1977, and its applicability to clinical inspection was declared around 1980; both happened in the USA [1-4]. MRI is now an indispensable medical tool throughout the world.

MRI is based on nuclear magnetic resonance (NMR), in which an atomic nucleus placed in a magnetic field absorbs the energy of radio waves of a specific frequency. MRI provides images of the distribution of hydrogen nuclei (protons) in the human body. The magnetic field strength of the MRI

Hitoshi Wada and Tsukasa Kiyoshi are with the National Institute for Materials Science, Sakura 3-13, Tsukuba 305-0003, Japan (e-mail: wada.hitoshi@nims.go.jp).

Masaki Sekino, Hiroyuki Ohsaki and Tatsuhiro Hisatsune are with the University of Tokyo, Kashiwanoha 5-1-5, Kashiwa 277-8561, Japan.

Hiroo Ikehira is with the National Institute of Radiological Sciences, Anagawa 4-9-1, Inage, Chiba 263-8555, Japan
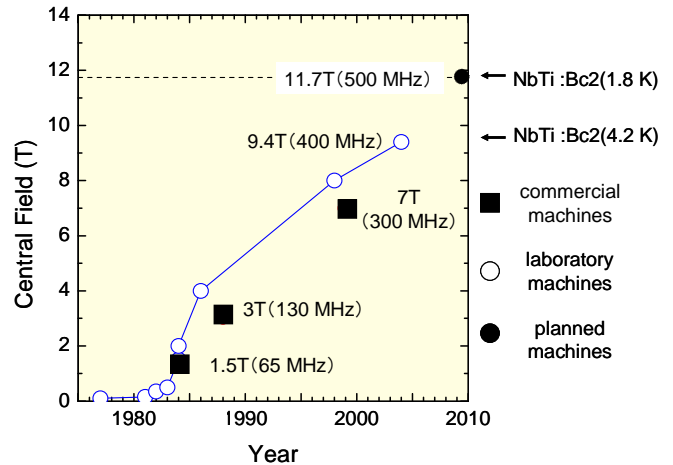
Fig. 1. Development of field strength of whole body MRI. 130 to 500 MHz indicate magnetic resonance frequencies of proton for respective fields.

magnets widely used in clinical settings is approximately 1.5 T (Tesla). When this strength is well increased, observation of much finer body structures and analysis of compositions of much smaller amounts become possible. An outstanding feature of MRI is that it allows non-invasive observation and diagnosis of organs; from the outside of the body without any damage to the body. This feature makes MRI applicable even to healthy people and highly effective for brain activity observation and brain function clarification. In other words, high-field MRI is a promising tool for understanding the human beings both physically and mentally in the aging society.

Fig. 1 shows the development of magnetic field strength of whole human body MRI where superconducting magnets usually have a bore diameter of ca. 900 mm. In addition to 1.5 T machines, 3 T machines have recently been admitted for clinical use in several countries and areas including Japan, USA and EU. Furthermore, 7 T machines are rapidly prevailing for research use and will probably be admitted for clinical use in the near future. These machines are all based on NbTi superconductors and operated at 4.2 K, liquid helium temperature. There are several 9.4 T machines in the world [5], but this is almost the upper limit field strength for NbTi at 4.2 K, as shown in Fig. 1. For higher fields, it becomes inevitable to either cool down the magnet to the superfluid helium temperature range or adopt a different kind of superconductor, that is Nb$_3$Sn. There are projects and plans in the world which are targeting whole body MRI machines to be operated at higher fields, such as 11.7 T (equivalent to proton resonance frequency of 500 MHz) [6]. The realization of these high-field MRI machines will need new, advanced superconducting magnet technology.

It is expected that high-field MRI will have extensive ripple effects on various industrial and educational developments, such as new diagnostic and therapeutic devices, new drugs, novel remedies for mental problems, supporting programs for
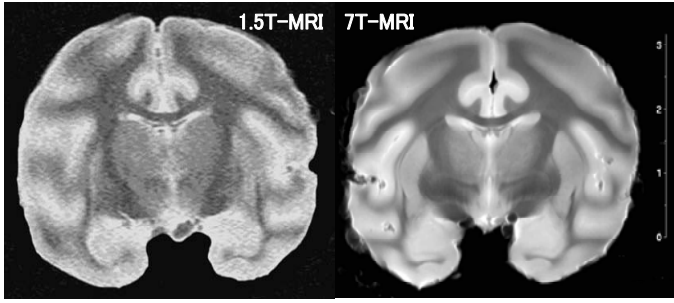
Fig. 2. Tomographic images of rhesus monkey's brain taken by a 1.5 T and a 7 T MRI machines. The 7 T machine gives much clearer image.
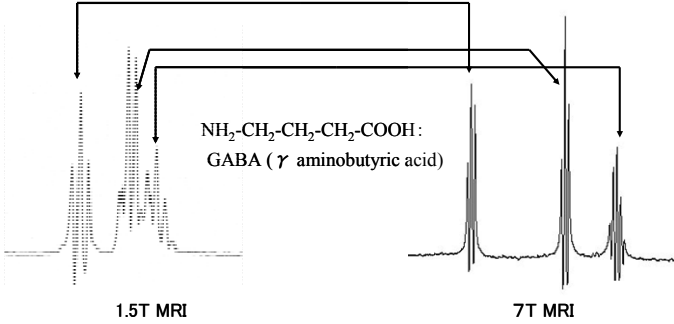

Fig3. Proton magnetic resonance spectroscopy (MRS) spectra of GABA at 1.5 T and 7 T. Chemical shift peaks are much more clearly separated at 7 T.

intellectual and physical trainings, and care-supporting robots that can communicate with humans.

II. EXPECTED PERFORMANCE OF HIGH-FIELD MRI

In MRI, NMR signals are converted into bright and dark spots forming images; stronger signals give brighter spots. Signals are taken from different positions in a human body, so that the resultant spots provide information related to shape, size and location of targeted body structures containing cancers, tumors, plaques, etc. Thus, the resolution and the sensitivity of MRI primarily depend on the strength of NMR signals.

Fig. 2 exhibits tomographic images of rhesus monkey's brain taken at 1.5 T and 7 T [7]. The 7 T MRI gives a much finer image than the 1.5 T MRI. Fig. 3 shows proton-MRS (Magnetic Resonance Spectroscopy) spectra of γ aminobutyric acid taken at 1.5 T and 7 T [7]. Much more detailed chemical shift peaks are obtained at 7 T.

The relationship between NMR frequency and magnetic field strength is given as follows:

$$\nu = \frac{\gamma B_0}{2\pi} \tag{1},$$

where ν is NMR (Larmor) frequency, γ magnetic rotation ratio and B_0 static magnetic field strength.

The origin of NMR signal is the resonant spin precession, the strength of which is proportional to B_0. When we discuss MRI performance, we should rather refer to the ratio of NMR signal strength (S) to noise strength (N). Also, S/N is a function of B_0.
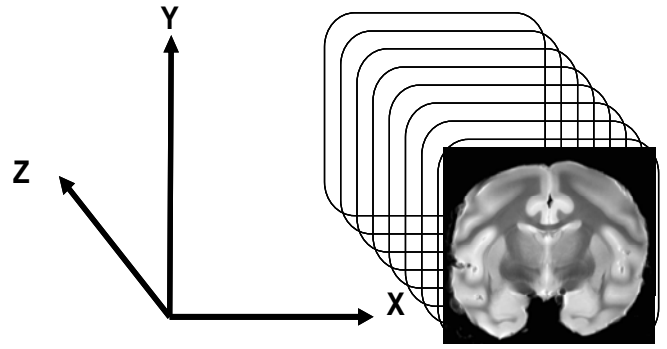

Fig. 4. Spatial resolution of MRI ; defined by 1 pixel length in the observed XY plane.

$$\left(\frac{S}{N}\right)_B = f(B_0) \tag{2}.$$

In an NMR measurement, there occur different noises from different sources that interfere with NMR signals; sample-coil impedances, high-frequency wave based field (B_1), etc. Then, S/N is given by the following relationship [8]:

$$\left(\frac{S}{N}\right)_B \propto \frac{\omega^2 \cdot B_1}{\sqrt{R_1 + R_2 + R_3}} \tag{3},$$

where $\omega = \gamma \cdot B_0$, $B_1 = f(\omega)$ and R_1, R_2 and R_3 are impedances related to ohmic loss, tissue loss and radiation loss, respectively. For a human or living body where tissue loss ($R_2 \sim \omega^2$) is dominant, relationship (3) is modified to be;

$$\left(\frac{S}{N}\right)_B \propto \frac{\omega^2 \cdot B_1}{\sqrt{\omega^2}} = \omega B_1 \propto B_0 \tag{4}.$$

To build up images or analyze the spectra, NMR signals need to be integrated. Thus, S/N is time dependent and integrated S/N is given as follows:

$$\left(\frac{S}{N}\right)_i \propto \sqrt{\text{data acquisition number} \cdot \left(\frac{S}{N}\right)_B} \propto B_0^{0.5} \tag{5}.$$

If the basic signal is stronger, the time duration to integrate certain signal strength is shorter. Or, for the same time duration integrated signal strength becomes larger at higher fields. Thus, integrated S/N depends on B_0 in an indirect manner.

We have estimated actual B_0 dependence of S/N by using the images in Fig. 2 and found the following relationship;

$$\left(\frac{S}{N}\right)_B \propto B_0^n \quad (n \geq 2) \tag{6}.$$

which we show in Fig. 5. There are engineering factors that may further increase S/N and exponent n; through the optimization of shimming coil, RF coil sensitivity, etc.

If we define spatial resolution as one pixel length in the observed plane of the image, as indicated in Fig. 4, it is given in the following relationship:
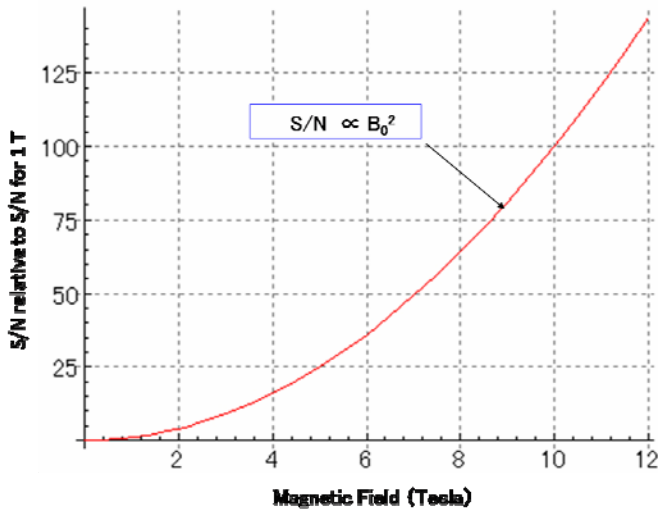
Fig. 5. Relative NMR S/N ratio as a function of magnetic field strength. S/N is defined to be 1 for 1 T.

Fig. 6. Estimated MRI performance relative to clinical MRI. Spatial resolution, mass sensitivity and data acquisition rate are based on ^{1}H imaging in Fig. 1.

Spatial Resolution, $f_S(B_0,t) \propto B_0^n$ $(n \geq 2.5)$ (7).

Similarly, sensitivity in terms of minimal detectable mass is given as follows:

Mass Sensitivity, $f_M(B_0,t) \propto B_0^n$ $(n \geq 2.5)$ (8).

Temporal and spectral resolutions may be represented by data acquisition rate which is the product of data acquisition number and time duration to build up sufficient signal strength. Thus, relationships (5) and (6) give data acquisition rate in the following manner:

Data Acquisition Rate, $f_{DAR}(B_0,t) \propto B_0^n$ $(n \geq 2.5)$ (9).

Relation (9) suggests that faster measurements become possible at higher fields.

MRI performance is based on spatial, temporal and spectral resolutions and mass sensitivity. It now seems reasonable for an engineering discussion about the prospect of high- field MRI to assume that MRI performance may in general be described in the following manner:

MRI Performance, $f_{MRI}(B_0,t) = f_{S,M,DAR}(B_0,t) \propto B_0^{2.5}$ (10).

As long as the performance of 1.5 T MRI machines for clinical use is regarded as the base for comparison, relationship (10) may be a good and conservative approximation.

Relying upon the semi-empirical relationships (6) and (10), we now try to estimate how far MRI performance is improved when the magnetic field strength is increased. Fig. 5 is based on relationship (6), showing relative NMR S/N ratio as a function of magnetic field strength. It is seen that S/N ratio is improved by a factor of 50 or more when the magnetic field strength is increased from 1 to 7 T. Such factor will be beyond 100 for magnetic fields above 10 T. This also means that MRS
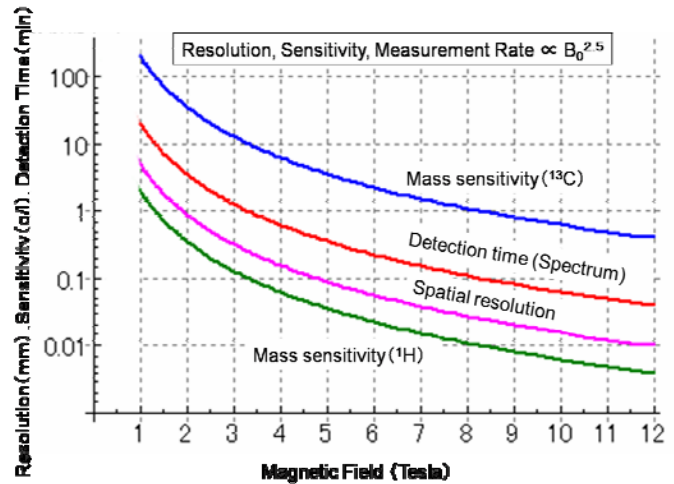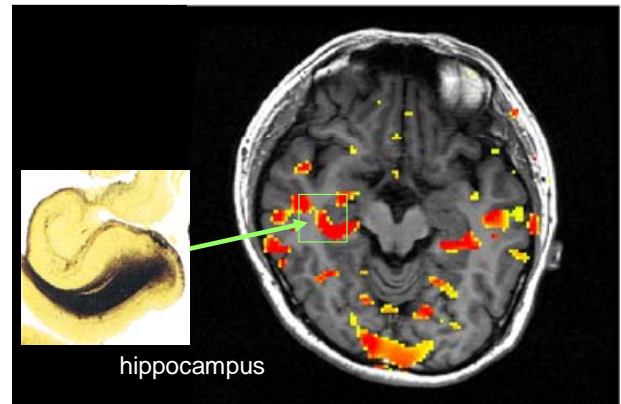

Fig. 7. Tomographic image of human brain taken at 3 T. The resolution is insufficient for clarifying Hippocampal activities.

measurement rate can become more than 100 times faster above 10 T.

Fig. 6 refers to relationship (10), summarizing estimated spatial resolution, mass sensitivity and data acquisition rate based on the S/N ratio data extracted from the images in Fig. 1. Around 3 T the spatial resolution reaches a level of 200 μm, which enables imaging of blood flow in fine vessels of brain. At 7 T the resolution may reach a level of 50 μm, which enables detection of small plaques, such as senile plaques at the early stage of Alzheimer's disease. Hippocampus is a tiny part of brain, and its activities are thought relevant to the memory function. Current clinical MRI machines cannot reveal details of these activities (Fig. 7). Therefore, a strong demand exists for high-field MRI in dementia research [9].

Fig. 6 predicts that the resolution may become a size of cells far above 10 T, when all engineering factors can be optimized. Fig.6 includes mass sensitivities based on ^{1}H- and ^{13}C- MRS. Carbon is an important component of bioorganic materials, and at well above 7 T the minimal detectable concentrations of ^{13}C fall into the range of milligram/litter which should make possible the in-vivo detections of such organic materials as plaques, dopamine, etc. Fig. 6 also indicates that at very high
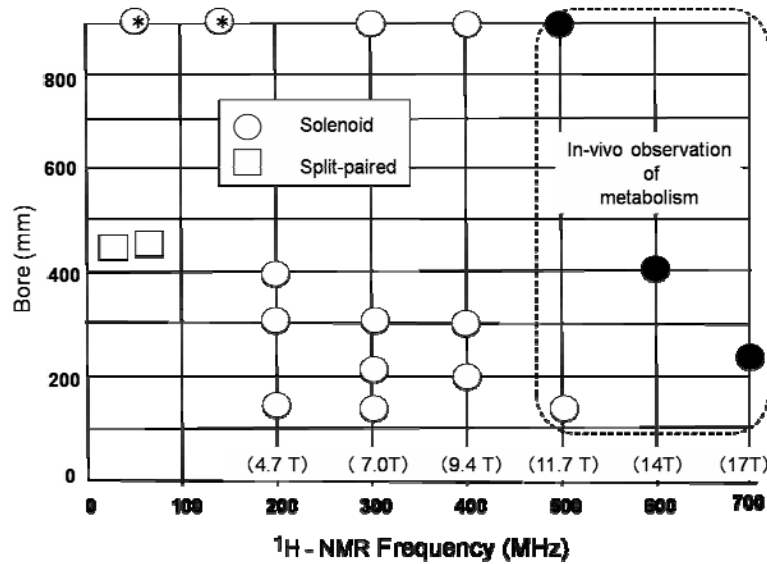
Fig.8. Existing and planned MRI machines in terms of magnet bore size and RF wave length/ magnetic field strength: * clinical; ○ commercial; ● proposed in different projects

TABLE I WHOLE BODY MRI MAGNET BORE SIZE, RF WAVE LENGTH, AND MAGNETIC FIELD STRENGTH

Sample	Coil dia.(mm)	Wave length (mm)*		Field(T)
		^{1}H	^{13}C	
human	∼ 900	60-100	250-400	11.7
monkey	∼ 400	50-80	200-300	14.1
rat	∼ 250	30-60	150-250	17.4

*RF wave length is the reciprocal of NMR frequency and the measure of distance RF can penetrate into body without substantial damping.
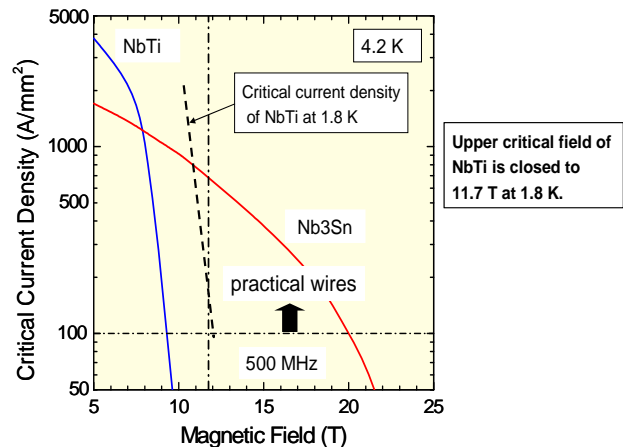

Fig.9.   Performance of NbTi and Nb$_3$Sn superconductors, candidate conductors for 11.7 T MRI magnet. NbTi needs to be cooled down below 4.2 K in order to generate magnetic fields higher than 10 T.

fields measurement rates can become 1,000 times larger than with conventional, clinical MRI. This should allow the detection of ^{13}C in the time range of milliseconds to tens of seconds, implying that some dynamic biological changes, such as metabolic reactions, may also be observed in-situ and in-vivo. One possible development out of this advantage would be in-vivo observation of regenerating process of transplanted tissues.

III.   11.7 T/500 MHZ MRI MAGNET

As described above, high fields can bring about many advantages including better MRI/MRS resolution, mass sensitivity and time efficiency. The most remarkable feature will be in that, since MRI and MRS based on ^{13}C NMR become possible in a quite practical (precise and enough fast) manner, in-situ and in-vivo observation on biochemical reactions or metabolism should be realized.

Fig. 8 demonstrates existing and planned MRI machines and Table I indicates the sizes and the field strengths of the magnets for ^{13}C NMR-based, in-situ and in-vivo MRI diagnosis on humans, monkeys and rats. If we try to measure metabolism, the ^{13}C NMR wave length which is the reciprocal of NMR frequency should be comparable with or larger than

the sample thickness so as to avoid the extensive damping of incident RF waves within the sample body. In the case of human body, the NMR wave length of proton, ^{1}H, should be larger than ~50 mm to penetrate the whole volume of human brain. Taking these requirements together with relationship (1) into account, the best set of MRI machines for achieving the most advanced and feasible imaging and spectroscopy will be 11.7 T (^{1}H NMR frequency of 500MHz)/900∅ for humans, 14.1T (600MHz)/400∅ for large animals and 17.4 T (750MHz) /250∅ for small animals. The magnets of Table I are all very challenging; especially the one for human is a real challenge, featuring the next generation high-field MRI. We now focus on 11.7 T/900 ∅ whole body MRI.

A. Superconductors

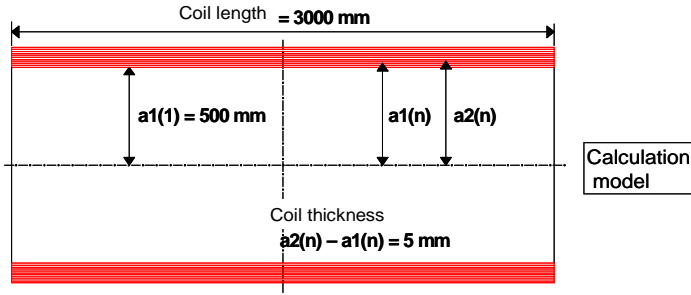NbTi superconductor has been used for whole body MRI

Fig.10. Coil model used for calculation of electromagnetic forces.

Fig.11. Volume of superconductor coil as a function of B^2. For fields 7 ~ 12 T, B^2 is proportional to stored energy in coil.

magnets due to its mechanical, electrical and economical advantages over other superconductors. However, its critical field is not much more than 10 T at 4.2 K, liquid helium temperature. Fig. 9 compares the performance of NbTi and Nb$_3$Sn, showing that 11.7T is beyond the limit of application for NbTi at 4.2 K. In order to reach 11.7 T, NbTi magnets need cooling down to superfluid helium temperature range, typically 1.8 K; we hereby assume from experience that practical superconductor wires should have a current density of 100 A/mm^2 or more.

It then seems reasonable to adopt Nb$_3$Sn for 11.7 T MRI; this will also make 4.2 K operation possible, since Nb$_3$Sn has its critical field far above 20 T. However, there are no whole body MRI magnets of Nb$_3$Sn yet. An 11.7 T machine may become the first chance for Nb$_3$Sn to be used for a whole body MRI magnet in persistent mode operation.

B. Electromagnetic Forces

In a single turn circular coil, the superconductor is subjected to hoop stress, σ_θ, as described below:

$$\sigma_\theta = Bjr \qquad (11)$$

where B is magnetic field experienced by the conductor, j current density, and r coil radius.

A whole body MRI magnet may be regarded as a modified NMR magnet with a very large bore. It is now possible to obtain an NMR magnet producing 23.5 T (1,000MHz) with a room temperature bore radius of 27 mm and an innermost coil radius of ca. 40 mm. In an 11.7 T (500 MHz) MRI magnet the generated magnetic field is only one half, but the coil radius becomes over 10 times larger. This means from (11) that σ_θ becomes 5 times larger in an 11.7 T magnet for the same j. Thus, electromagnetic force is a serious limiting factor to MRI magnets and we need conductors of high mechanical strength. In the design of high field NMR magnets, hoop stress typically assumed is at a level of 200 MPa. If we take the same number for the design of an 11.7 T/900∅ magnet, allowable current density is around 38 A/mm^2. This is why NbTi attracts magnet engineers even at 11.7 T, although high-field NMR magnets consist of NbTi plus Nb$_3$Sn conductors.

To estimate electromagnetic forces induced in an 11.7 T MRI magnet, we use a coil model shown in Fig. 10 [10]. In this model the followings are fixed:
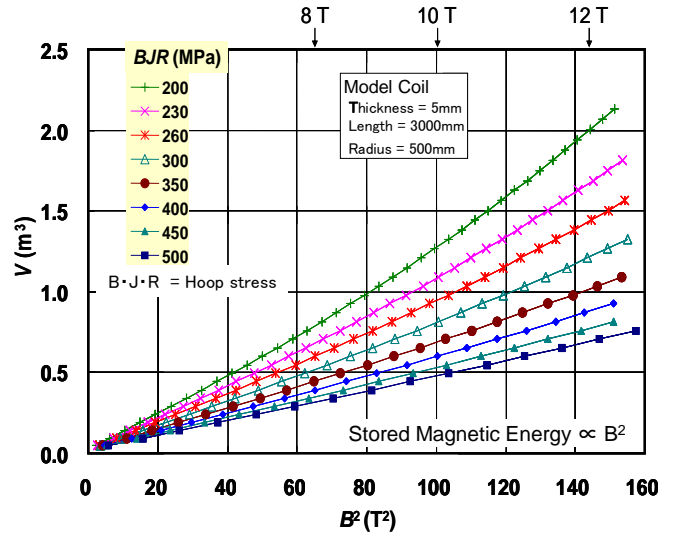
- Inner radius of the innermost layer coil , a1(1) = 500 mm.
- Layer thickness, a2(n)-a1(n) = 5 mm.
- Coil length = 3,000 mm.

Notations a1 and a2 refer to the inner and the outer radius of each layer, respectively. The whole coil consists of layers 1, 2, 3 to N. The current density of each layer is so determined that the calculated hoop stress based on (11) does not exceed a set value. We need to take into account the increment in the hoop stress for layer n by the magnetic field generated by the outer next layer n+1; current densities for inner layers are decreased.

In the calculation the set σ_θ values range from 200 - 500 MPa. Fig. 11 indicates the relationship between magnetic field and magnet volume for each of these set values. With the upper limit of hoop stress being 200 MPa, the magnet volume becomes larger by a factor of 1.5 or more, when magnetic field is increased from 10 to 12 T. It should be noted that this drastic increase of magnet volume is moderated for larger set values.

Thermal disturbances due to wire motions are emphasized with increasing electromagnetic forces, which will suppress the upper limit of acceptable hoop stress in a metallic superconductor magnet. Mechanical stability of conductors will play a decisive role, and there may be a chance for Hastelloy tape reinforced ReBCO oxide superconductors to be used at a hoop stress level of 500 MPa. Although ReBCO and some other oxide superconductors seem promising in terms of electromagnetic forces, they apparently have many problems to be overcome when applied to MRI; coiling techniques to ensure field homogeneity, field decay due to joining, long-term magnetic instability due to magnetization, etc.

C. Possible Design of 11.7 T MRI Magnet

Possible designs of 11.7 T MRI magnet to be operated in persistent mode are shown in Fig. 12. When the central field strength is 11.7 T, the maximum field experienced by the superconductor coils becomes ca. 12 T. Two designs were
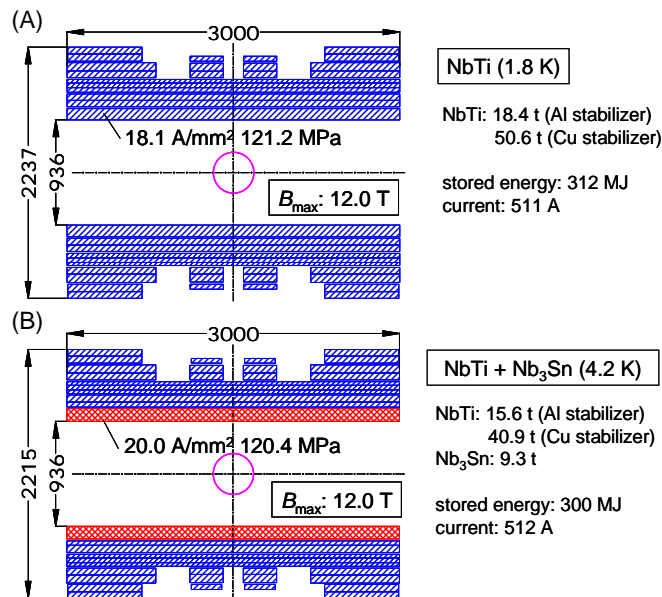
(A)

3000

2237

936

18.1 A/mm² 121.2 MPa

B_{max}: 12.0 T

NbTi (1.8 K)

NbTi: 18.4 t (Al stabilizer)
50.6 t (Cu stabilizer)

stored energy: 312 MJ
current: 511 A

(B)

3000

2215

936

20.0 A/mm² 120.4 MPa

B_{max}: 12.0 T

NbTi + Nb₃Sn (4.2 K)

NbTi: 15.6 t (Al stabilizer)
40.9 t (Cu stabilizer)
Nb₃Sn: 9.3 t

stored energy: 300 MJ
current: 512 A

Fig.12. Coil structure designs of 11.7 T magnets

Ø 900
Ø 2897

3777

3338

Fig.13 A design example of unshielded 11.7 T MRI magnet (NbTi + Nb₃Sn). .

Fig.14. Stray field distribution of 11.7 T/900∅ NbTi magnet .

examined:
  Design-A: 11.7 T solenoid made of NbTi;
    operation temperature = 1.8 K;
    no cooling channels in the coils.
  Design-B: 11.7 T solenoid made of NbTi and Nb₃Sn;
    operation temperature = 4.2 K;
    no cooling channels in the coils.
For both cases the inner diameter of coils was assumed to be 936 mm so that the room temperature bore could be 900 mm. Furthermore, the following values were assumed;
• maximum coil length = 3,000mm;
• field homogeneity < 1 ppm for 360 mm DSV (diameter sphere volume);
• I_{op}, operation current ($< 0.6\ I_C$) = 500 A.
As a result of these assumptions, the field homogeneity is 0.7 ppm for design-A, while it is 0.61 ppm for design-B. The operation current was assumed to be 500 A which is a typical number for ordinary persistent current switches, and may thus vary depending upon the switches to be used. For persistent mode operation, I_{op}/I_C is set to be less than 0.6. For design A, I_{op}/I_C becomes 0.44 for the innermost coil and less than 0.47 for any coil of the magnet. The maximum hoop stress experienced by the coils is 121.2 MPa.

  In the case of design B, I_{op}/I_C is only 0.28 for the innermost coil, since it adopts a Nb₃Sn coil. However, the maximum I_{op}/I_C reaches 0.52 for the NbTi coils since the magnet is operated at 4.2 K. The maximum hoop stress experienced by the coils is 120.4 MPa.

  There is no substantial difference in magnetic energy stored in design-A and design-B magnets. In order to reduce the weight of conductors, aluminum stabilizer may be a good choice as indicated in Fig. 12.

  Fig. 13 is one example design of an 11.7 T magnet to be operated at 4.2 K without magnetic shielding.

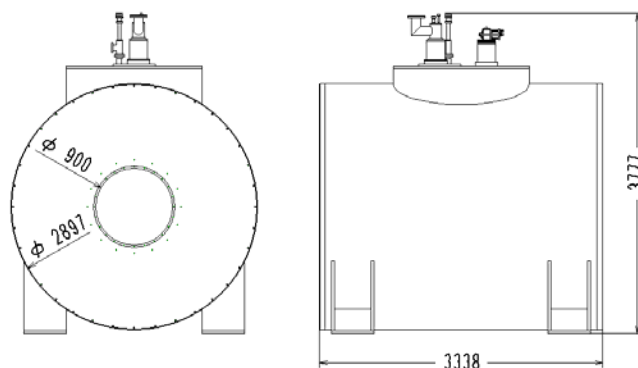   Compared with a liquid helium cooled magnet in persistent mode operation, a design-A MRI magnet requires a more complicated cryostat for superfluid helium cooling, consumes more helium and needs more operation costs due to the safety measures against power breakdown, etc. We believe the current magnet technology can realize this design of MRI magnet, but 11.7 T is the limit. Higher field will surely require coils made of Nb₃Sn or other superconductors, such as high temperature oxide superconductors.

  Use of Nb₃Sn makes a design-B magnet a difficult one. If the Wind & React method is adopted, a huge heat-treatment furnace is needed for 936 mm diameter coil. Superconducting joints with NbTi conductors must be quite long for straight overlapping, due to the brittleness of Nb₃Sn. On the other hand, design-B magnet fabrication based on the React & Wind method requires an extremely precise control of strain over the whole fabrication process. Application of either method definitely needs a fair amount of R & D in advance of actual magnet fabrication. Once the fabrication process is established, it will be applicable to MRI magnets generating even higher fields than 11.7 T.

  In the above discussion active shielding is not included, since the fabrication of an 11.7 T superconducting magnet itself is very difficult. Fig. 14 indicates an estimated stray field distribution of a design-A 11.7 T/900 mm∅ magnet. The so-called 5 gauss line along the central axis, or z-direction, lies 32 m away from the center of the magnet. Thus, some magnetic
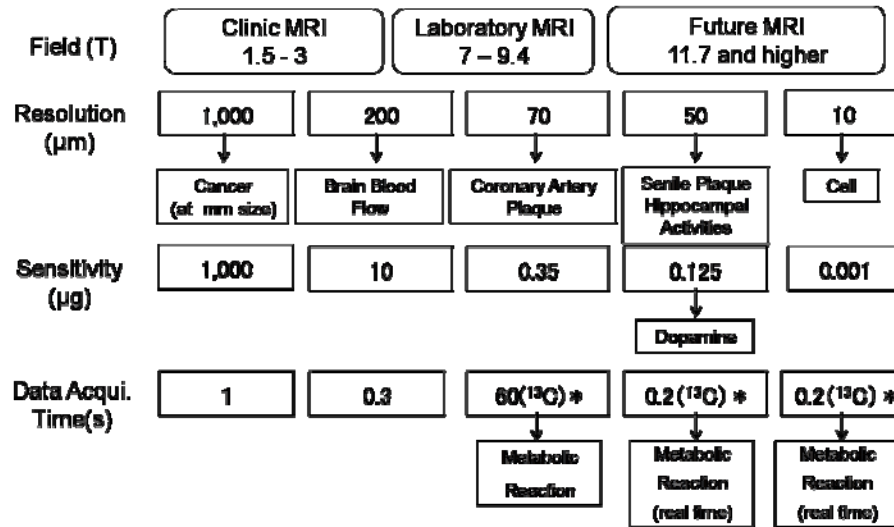
Field (T)	Clinic MRI 1.5 - 3		Laboratory MRI 7 – 9.4		Future MRI 11.7 and higher	
Resolution (μm)	1,000	200	70	50	10	
	Cancer (at mm size)	Brain Blood Flow	Coronary Artery Plaque	Senile Plaque Hippocampal Activities	Cell	
Sensitivity (μg)	1,000	10	0.35	0.125	0.001	
				Dopamine		
Data Acqui. Time(s)	1	0.3	60(^{13}C) *	0.2(^{13}C) *	0.2(^{13}C) *	
			Metabolic Reaction	Metabolic Reaction (real time)	Metabolic Reaction (real time)	

Fig. 15. Summarized MRI performances based mainly on ^{1}H-NMR. Future MRI may enable in-situ observation of metabolic reactions based on imaging and spectroscopic analysis based also on ^{13}C-NMR.

shielding is indispensable to high-field MRI at this level. Shielding by ferromagnetic material wall will need more than 500 tons of steel, which may however not be quite nonsense in relation to the expected total construction cost of an 11.7 T MRI system. There is no doubt active shielding is much preferred with this system not only at hospital but also in research laboratory.

IV. PROSPECT

A. Progresses and New Applications to Occur

Fig. 15 summarizes the performances of MRI operated at different magnetic field strengths. At very high fields, such as 11.7 T, resolution, sensitivity and measurement rate are so enhanced that very fine lesions as well as biochemical reactions become detectable. Then, cancer, dementia, myocardial infarction, diabetes and other serious diseases could be treated at a much earlier stage than now, which should result in less burden to human organism.

MRI machines can be classified into tunnel type and open type in terms of magnet configuration. The tunnel type includes a single solenoid magnet, while the open type consists of a split-paired magnet. For both types the relative direction of magnetic field to human body is either parallel or perpendicular. Fig. 16 shows these 4 types of MRI machines. There is strong demand for high-field machines of all these types. Type (a) is the most popular machine and the first 11.7 T machine will be of this type.

If the performance of 11.7 T MRI lives up to our expectation, a tremendous progress will take place in medicine that may be regarded as a paradigm shift. Since very small lesions could be detected, cancer, cerebral tumor, myocardial infarction and many other life-style related diseases with high mortality might be found and treated at very early stage. The detection of senile plaques at very early stage should greatly enhance the effect of medication on Alzheimer's disease or dementia. The ^{13}C NMR based MRS will identify the carbohydrate metabolism, leading to more specific remedies against diabetes. All these benefits, should result in the essential reduction
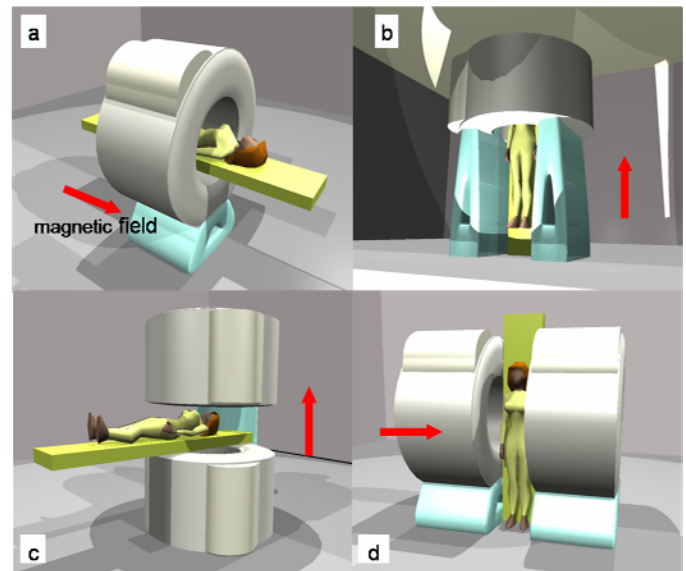

Fig. 16. 4 Types of MRI machines in terms of magnet configuration and relative direction of magnetic field to human body:
(a) tunnel, parallel/horizontal filed,
(b) tunnel, parallel/vertical field,
(c) open, perpendicular/vertical field,
(d) open, perpendicular/horizontal

of health care expenditures which can otherwise be a heavy burden to the national budget in most of the countries.

Types (c) and (d) have been developed for use in image-guided therapy [11,12]. These geometries enable surgeons to easily access lesions. Real-time images are provided to show the relative location between the lesion and surgical instruments. At higher fields, however, the most remarkable applications of types (b) – (d) could occur in the area of so-called functional MRI (fMRI). Open type (c) and (d) machines accept an examinee in much less constrained way than tunnel type machines and allow them to have sight. Then, brain scientists can give their examinees a much larger variety of stimuli than with a tunnel type machine. The type (d) is the
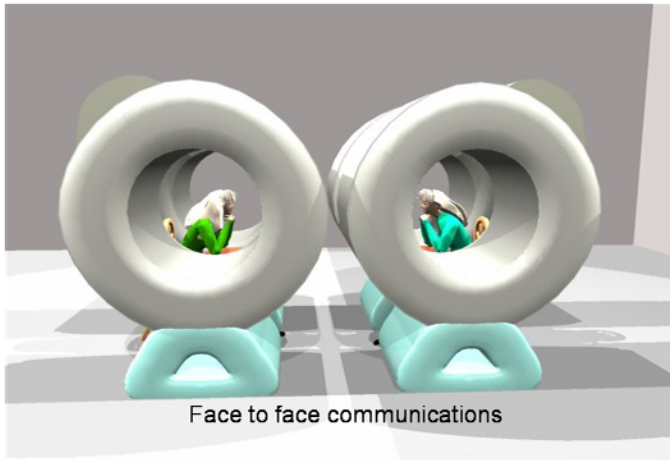
Fig. 17. fMRI for communication science consisting of 2 open MRI machines. 2 patients or examinees facing each other have conversation, and their brain activities are in-situ analyzed by functional MRI.

TABLE II MULTI NUCLEI MRI/MRS.

^{13}C	Metabolism of carbohydrate and fat
^{17}O	Metabolism of oxygen
	Blood flow observation
^{1}H	Metabolism of cerebral amino acid in brain
	Analysis of neurotransmitter
^{19}F	Analysis of cancer medication effect
	Metabolism of anticancer drug
	Diagnosis of Alzheimer's disease

least popular machine today, but will attract a great number of cognition scientists, physicians and psychologists. Fig. 17 illustrates an example of application of type (d) in a conceptual way. Two type (d) machines are so set up that two examinees can communicate with each other in face to face manner. Then, brain activities and functions are in-situ inspected on the basis of fMRI. The possible outcome of this application will be a variety of programs for educational trainings, psychotherapies, etc.

High-field MRI/fMRI will create innovations in all kinds of industries including medicine, food, education, cosmetics, energy, environment, etc.

From the magnet technology point of view, high-field, split-paired MRI magnets are another tough challenge due to huge and non-symmetrical electromagnetic forces plus those high fields that superconducting coils actually experience. In addition, magnetic shielding of such large split-paired magnets will require new technical steps.

An interesting design of MRI magnet has been proposed where the homogeneous field range is not at the center but off the center of the magnet [13]. If this magnet is used in the type (b) MRI machine, the examinee sitting beneath the coil can have some sight, so that he may be able to carry out some task such as reading or drawing. Then, the MRI of such magnet configuration would be highly supportive of the Benton Visual Retention Test widely adopted on suspected dementia patients [14].

Table II shows multi nuclei MRI/MRS that becomes more effective at higher fields. For example, ^{19}F MRS will reveal the metabolism of anticancer drugs, proving their efficacy. This can lead to optimizing the medication and minimizing the very strong side effects anticancer drugs usually cause. In addition, ^{19}F-labelled molecular probes can be used to detect amyloid beta plaques in the brain [15]. This technique potentially leads to a new diagnostic method for Alzheimer's disease.

B. Toward Higher Fields

As is shown in Fig. 8, magnetic field strengths up to 3 T have been admitted at hospital, and 7 T will probably be accepted in some countries rather soon. For animals, 17 T MRI is now available in which Nb_3Sn conductors are used. For these extremely high fields, high-field MRI may strongly be correlated with high-field NMR in terms of superconductor development. In fact, it was at 11.7 T (500 MHz) that Nb_3Sn conductors started to be used for NMR magnets.

Recent progress made in superconductor technology may provide further options for MRI machines to be operated at 11.7 T and higher fields.

MgB_2 has already been used to test a conduction-cooled, open type magnet suitable for a whole body MRI machine [16]. This magnet was operated at 0.5 T in powered mode. The application of MgB_2 to high-field MRI, however, needs a substantial improvement of superconducting properties at high fields.

Nb_3Al is also promising for high-field MRI use, since this superconductor is known to be stable against strain and thus electromagnetic force. The fact that superconducting joint with NbTi has already been established makes Nb_3Aly attractive for whole body MRI use [17].

A 3 T MRI system for head imaging is under development in which mechanically reinforced Bi-2223 oxide superconductor is used [18]. The ReBCO superconductor formed on a Hastelloy sheet has very high mechanical strength over 500 MPa. As shown in Fig. 11, high mechanical strength of superconductor can greatly reduce the magnet volume, and moderate design requirements.

Persistent mode operation is a difficult hurdle for these new superconductors when applied to MRI, primarily because the fabrication of superconducting joints is not yet possible for such superconductors. Recently, powered mode operation is gaining interest by magnet engineers, and the 0.5 T MRI of MgB_2 mentioned above has adopted powered mode operation. This new approach to MRI operation will widely be adopted as new superconductors with much better properties are developed.

Since Bi-2223 and ReBCO superconductors are tape conductors, solenoid coil fabrication is difficult. When these conductors are adopted, pancake type winding will be the choice for coil fabrication. However, all the MRI magnets so far fabricated are based on solenoid coils. In the case of pancake type winding, the number of superconducting joints will tremendously be increased, which makes MRI magnet fabrication to be operated in persistent mode more difficult. In this respect, an interesting report exists on a 500 MHz NMR solenoid magnet development where a Bi-2223 conductor reinforced by a bronze tape was wound into a solenoid inner

coil [19]. This 500 MHz system was operated in powered mode and showed NMR measurement performance comparable with that in persistent mode. On the other hand, this system suffered a long time lasting drift due to the shielding current of the Bi-2223 coil. The same problem will probably happen to ReBCO conductors, too.

C. Contribution of Magnet Technology

A leading project, Iiseult/INUMAC project, is proceeding in France, where an 11.7 T whole body MRI magnet is under development [6]. This ambitious magnet has adopted NbTi conductor, double pancake-type winding, active shielding and powered mode operation at 1.8 K, thus including many technical challenges. There are similar activities in other places of the world, Korea, Japan, US, etc.

High-field MRI will no doubt have a great impact on the medicine of the 21st century and the aging society. Magnet technology can contribute to the progress of high-field MRI in two ways; (1) by developing MRI magnets for higher fields and (2) by developing of new design-based MRI magnets for new applications.

REFERENCES

[1] P. C. Lauterbur, "Image formation by induced local interactions: examples employing nuclear magnetic resonance," Nature, vol. 242, pp. 190-191, 1973.
[2] P. Mansfield and A. A. Maudsley, "Medical imaging by NMR," *Br. J. Radiol.,* vol. 50, pp. 188-194, March 1977.
[3] W. A. Edelstein, J. M. Hutchison, G. Johnson, and T. Redpath, "Spin warp NMR imaging and applications to human whole-body imaging," *Phys. Med. Biol.*, vol. 25, pp. 751-756, July 1980.
[4] F. W. Smith, J. M. Hutchison, J. R. Mallard, G. Johnson, T. W. Redpath, R. D. Selbie, A. Reid, and C. C. Smith, "Oesophageal carcinoma demonstrated by whole-body nuclear magnetic resonance imaging," *Br. Med. J.*, vol. 282, pp. 510-512, February 1981.
[5] T. Vaughan, L. Delabarre, C. Snyder, J. Tian, C. Akgun, D. Shrivastava, W. Liu, C. Olson, G. Adriany, J. Strupp, P. Andersen, A. Gopinath, P.F. van de Moortele, M. Garwood, and K. Ugurbil, "9.4T human MRI: Preliminary results," *Magn. Reson. Med.*, vol. 56, pp. 1274-1282, December 2006.
[6] P. Vedrine, G. Aubert, F. Beaudet, J. Belorgey, J. Beltramelli, C. Berriaud, P. Bredy, Ph. Chesny, A. Donati, G. Gilgrass, G. Grunblatt, F.P. Juster, F. Molinie, C. Meuris, F. Nunio, A. Payn, L. Quettier, J.M. Rey, T. Schild, and A. Sinanna, "The whole body 11.7 T MRI magnet for Iseult/INUMAC project," *IEEE Trans. Appl. Superconduct.*, vol. 18, pp. 868-873, June 2008.
[7] National Institute of Radiological Science Press report HP http://www.nirs.go.jp/news/press/2004/11_19.shtml, November 2004.
[8] D. Hoult, "Sensitivity of the NMR Experiment; Encyclopedia of Nuclear Magnetic Resonance," vol. 7, pp.4256-4266, edit. John Wiley
[9] D. Le Bihan, "Looking into the functional architecture of the brain with diffusion MRI," *Nat. Rev. Neurosci.*, vol. 4, pp. 469-480, June 2003.
[10] A. Otsuka and T. Kiyoshi, "High-field magnet design under constant hoop stress," *IEEE Trans. Appl. Superconduct.*, vol. 18, pp. 1529-1532, 2008.
[11] W. A. Hall and C. L. Truwit, "Intraoperative MR-guided neurosurgery," *J. Magn. Reson. Imaging*, vol. 27, pp. 368-375, February 2008.
[12] J. F. Schenck, F. A. Jolesz, P. B. Roemer, H. E. Cline, W. E. Lorensen, R. Kikinis, S. G. Silverman, C. J. Hardy, W. D. Barber, E. T. Laskaris, et al. "Superconducting open-configuration MR imaging system for image-guided therapy," *Radiology*, vol. 195, pp. 805-814, June 1995.
[13] H. Zhao, S. Crozier, and D. M. Doddrell, "Asymmetric MRI magnet design using a hybrid numerical method," *J. Magn. Reson.*, vol. 141, pp. 340-346, December 1999.
[14] M. Sekino, H. Ohsaki, H. Wada, T. Hisatsune, O. Ozaki, and T. Kiyoshi, "Fabrication of an MRI model magnet with an off-centered distribution of homogeneous magnetic field zone," to appear in Proc. MT21, *IEEE Trans. Appl. Superconduct.*
[15] M. Higuchi, N. Iwata, Y. Matsuba, K. Sato, K. Sasamoto, and T.C. Saido, "^{19}F and ^{1}H MRI detection of amyloid beta plaques in vivo," *Nat. Neurosci.*, vol. 8, pp. 527-533, April 2005.
[16] M. Modica, S. Angius, L. Bertora, D. Damiani, M. Marabotto, D. Nardelli, M. Perrella, M. Razeti and M. Tassisto, "Design, construction and tests of MgB$_2$ coils for the development of a cryogen free magnet," *IEEE Trans. Appl. Superconduct.*, vol. 17, pp. 2196-2199, June 2007.
[17] T. Fukuzaki, H. Maeda, S. Matsumoto, S. Yokoyama and T. Kiyoshi, "Study of joint resistance in Nb$_3$Al-NbTi superconducting joint for high field NMR," *IEEE Trans. Appl. Superconduct.*, vol. 17, pp. 1435-1437, June 2007.
[18] H. Kitaguchi, O. Ozaki, M. Hamada, N. Ayai, K. Sato, S. Urayama, and H. Fukuyama, "Development of a Bi-2223 HTS Magnet for 3T MRI System for Human Brains," Presented at MT-21.
[19] T. Kiyoshi, M. Hamada, M. Hosono, M. Takahashi, T. Yamazaki, and H. Maeda, "HTS-NMR: Present status and future plan," Presented at MT-21.